NDT.net - The e-Journal of Nondestructive Testing (December 2008)
For more papers of this publication click: www.ndt.net/search/docs.php3?MainSource=25

Using Drilled Holes as Reference in Magnetic Flux Leakage Measurements: An Investigation Based on Finite Element Modelling

Till Schmitte[1], Ashraf Koka[2]

[1]Salzgitter Mannesmann Forschung GmbH, Duisburg, Germany
[2]Vallourec Mannesmann Deutschland GmbH, Düsseldorf, Germany

Abstract
In order to have a fast recalibration method of magnetic flux leakage (MFL) inspection systems it is proposed to use a drilled hole as the reference. The hole can be drilled in the pipe end region which will be cut in further production. The fast recalibration is important if quantitative testing including defect separation is required but small lot sizes would normally lead to very frequent calibration cycles. In this work we present a calculation of MFL signals of standard notches and drill-holes with the goal of finding a corresponding calibration scheme. The work is based on finite element modelling (FEM). As result we show that it is indeed possible to assign equivalent drill-holes to a specified notch-depth, however, only for a certain range of parameters. This range depends mainly on the sensor lift-off.
Keywords: Magnetic Flux Leakage, FEM

1. Introduction

Magnetic flux leakage (MFL) as a non-destructive testing method is a valuable tool in seamless tube production. MFL is a cheap, because dry and fast, method and is frequently integrated into multiple test benches used for inline and offline NDT based process control and acceptance procedures.
Salzgitter Mannesmann Forschung GmbH (SZMF) is intensively working on many aspects of MFL, such as sensor system (introduction of GMR sensors), inside-outside defect separation (new sensor arrangements), data analysis and denoising (wavelet techniques) [1] and signal modelling (FEM methods) [2]. As an essence of this work SZMF designed and built a testing system for pipe end testing in Rath works (plug mill) of Vallourec-Mannesmann [3].
During the commissioning phase of the pipe end testing system [3] it turned out that it may be desirable to check the machine parameters without actually recalibrating the system using the attached but offline situated calibration stand. However, it is impossible to place a test notch during production and usually impracticable to insert a test pipe into the production flow. In addition, the signal amplitude of MFL is depending on material properties, in particular on the saturation B-field, and on the pipe geometry. Therefore it may be necessary to have a calibration tube for every material / geometry combination which would lead to extraordinary effort.
The idea emerged to use drilled holes as a reference, because it may be possible to drill a hole into a production pipe in the end region (to be cut) as a method for having a reference defect for online calibration, without disturbing the production flow too much. However, in order to use drilled holes as reference it is necessary to know the correspondence of signal amplitudes to usual test notches. Therefore, an investigation was launched with the aim of finding a simple functional relation. The investigation was performed using Finite Element Modelling (FEM) in combination with a special software module for electromagnetic calculations.

Previous work of our department in this field was related to FEM based calculations of MFL signals in a 2d model [2]. Here we present results using a full 3d model of the magnetization setup and a reduced 3d model of the defect.

2. Finite Element Modelling

2.1. Magnetization setup

In a first step the magnetizing setup was modelled. The geometry of the magnet poles and the angle of the magnetic poles to the pipe were taken from original technical drawings of the pipe end inspection system. The sensor is placed exactly between the two magnetic poles at a distance called "lift-off", *d*, below the pipe surface.

The actual model takes advantage of two planes of symmetry of the setup: first, the model has a plane of symmetry perpendicular to the pipe axis cutting the magnetic poles in halves. This symmetry imposes the constraint of parallel flux lines to this plane. Second, the model has a symmetry plane through the pipe axis which parts the magnetizing setup in equal halves. The constraints for this plane are perpendicular flux lines.

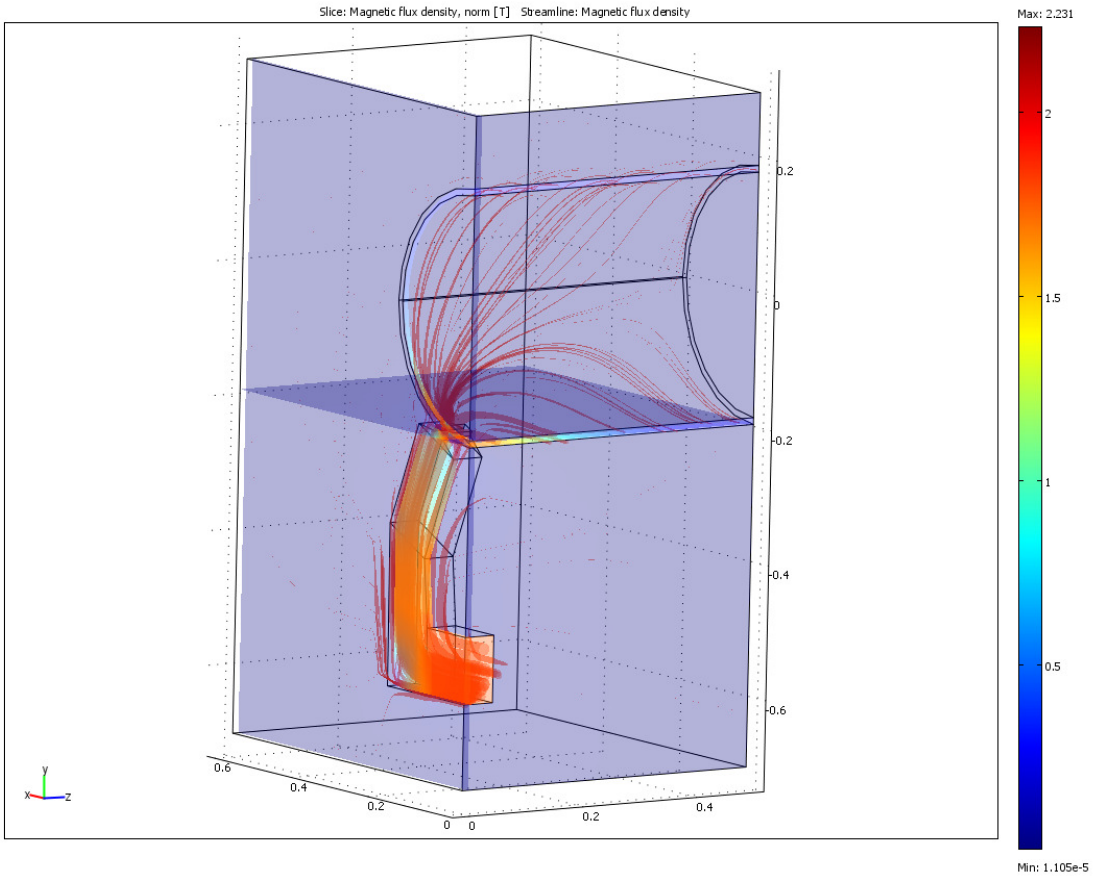

Figure 1: 3d model of the magnetizing setup and pipe of the pipe end inspection system. The plot shows only one quarter of the real part, because symmetric regions are not modelled, seen main text. The sensor position is exactly on the front edge of the above plot, below the pipe surface. As a solution of the 3d model of the magnetizing setup some flux lines are shown.

An important issue for building a realistic model is to decide for right length of the pipe. It is clearly seen from the solution in *Figure 1* that the flux lines are not confined to the region of the pole shoes – they extend to the region besides the magnet. For MFL this also means that in the presence of a defect the flux is not only deviated outside the pipe wall (and can be measured) but is also redirected inside the pipe wall in regions besides the actual defect. This is essentially the reason why it is so important to use 3-dimensional models instead of 2-dimensional ones. The pipe length is reduced in the model compared to reality, but it was checked that the limited length does not have any influence on the flux density in the pipe region beneath the sensor.
Material parameters (permeability, μ) have to be assigned to the different parts of the model. In order to find good correspondence with the real situation, it is important to model using non-linear magnetic materials, i.e. μ_r is a function of the magnetic flux density, $\boldsymbol{B}$: $\mu_r=\mu_r(|\boldsymbol{B}|)$. The magnetic field source is chosen such that the magnetic flux density in the gap between pole shoe and pipe shows realistic values. The FEM calculations are done using the software COMSOL [4] in the magnetic quasi-static 3D application mode, thus we solve for the vector-potential $\boldsymbol{A}$.

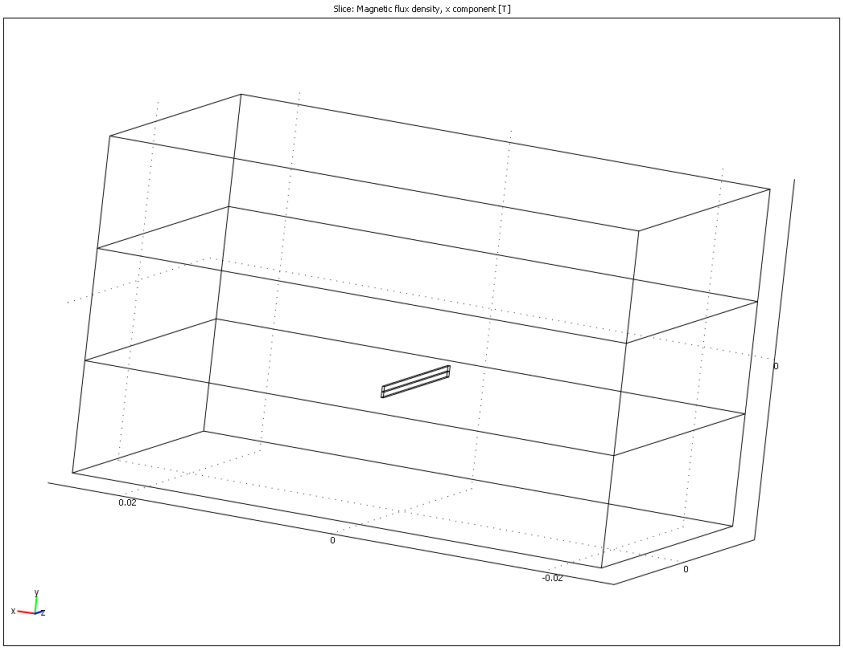

Figure 2: reduced model used for stray flux calculation. The middle part is the ferromagnetic material with a remanent field extracted from the solution of the large model. The upper and lower part is air. The defect is a rectangular notch.

2.2. Simulation of Defects

After solving the model for the magnetization setup, defects are introduced as a small disturbance to the system.
Practically we chose a rectangular plate of the appropriate non-linear material, which represents the pipe wall in the region of the sensors. In order to have a realistic situation we extract the flux density of the large model in this region, $\boldsymbol{B}=\boldsymbol{B}(\boldsymbol{r})$. As $\boldsymbol{B}$ is a 3d vector field it is necessary to know the course of all components of B in all space dimensions. In the model of the magnetization setup the flux density inside the pipe is best

represented in cylindrical coordinates. When "bending" the pipe wall to the plate form, the necessary coordinate transform is easily done by: $B_\phi=B_x$, $B_r = B_y$, $B_z=B_z$. The main flux direction inside the pipe wall near the sensor position is in the large model along ϕ and in the plate model along x and it turned out that this field component is actually the only relevant. Therefore we measured the field in the large model and approximated the course of the flux density with a 6^{th} order polynomial. Again we found that only one space coordinate is relevant, which is z, the direction parallel to the pipe axis, i.e. we have $B_\phi = B_x(z) = a_0 + a_2*z^2 + a_4*z^4 + a_6*z^6$.
After extracting the data and fitting the coefficients a_i the interpolated field is taken as the remanent flux density of the plate. This procedure results in a small model and thus fast computing time is gained where at the same time the magnetic flux distribution is quite realistic.
The defects are now modelled as missing material in this plate. An example is displayed in *Figure 2*. Another advantage of this reduced model is that outside and inside defects are calculated simultaneously – by just switching the plane in which the sensor moves from one side of the plate to the other.
The simulated signals were compared to measured signals and a good correspondence was found. However, the signal amplitude strongly depends on the actual material parameters and correspondence could only be reached if the assumed B-H loop in the FEM calculations is modelled from hysteresis measurements of the material under test.

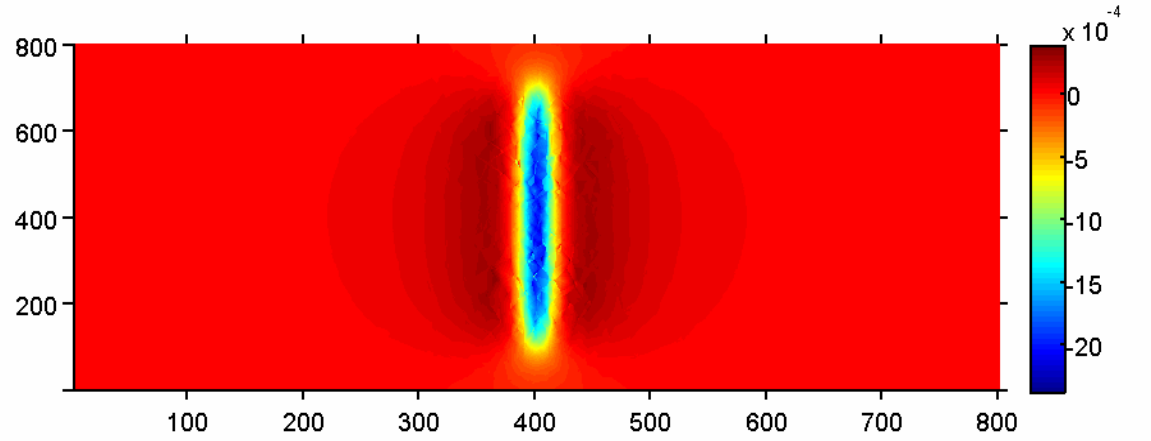

Figure 3: result of the FEM calculation of a 10% outside notch. The wall thickness is 10 mm, the notch width is 0.1 mm and the notch length 15 mm. In the plot the x-component of the magnetic flux density is plotted as a function of space coordinates x (circumference) and z (pipe length).

2.3. Sensor Signals

The new pipe end inspection [1,3] setup is equipped with GMR sensors. The actual measured signal of such sensor is directly proportional to the magnetic flux density, because the signals are calibrated and temperature corrected by the digital signal processor units of the installation. In addition, as the geometry of the sensor is point-like, it is not necessary to take sensor characteristics into account.
The simulation as it is described in the forgoing section results in the complete vector field $\boldsymbol{B(r)}$. For visualization it is necessary to plot only one component of $\boldsymbol{B}$ in one cross-section of the solution space. This is exemplarily shown in *Figure* 3 for B_x (the

main field direction) in a plane at a distance of 1 mm above the steel-plate. This distance is the lift-off distance of the sensor.
In addition, the pipe end testing machine in Rath features a system for inside/outside defect localization which uses two rows of sensors, both measuring the circumferential component of the ***B***-field but exhibiting a different lift-off. The first GMR-row has a lift off of 1mm (*S1*), the second of 2.67mm (*S2*).

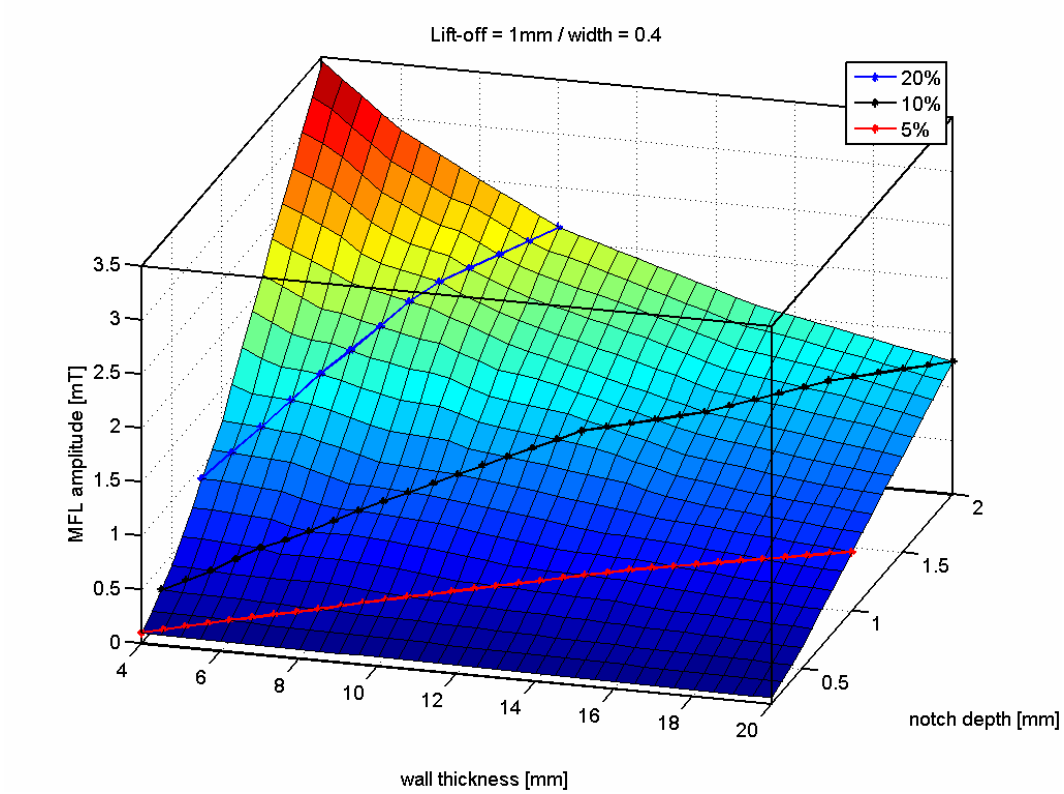

Figure 4: simulation results for the signal *S1* as a function of notch depth, *b*, and wall thickness, *t*.

3. Results

3.1. Simulated Case

Generally the signal amplitude depends not only on the defect (notch depth, width, length / drill-hole diameter) but also on geometry parameters of pipe and setup (wall thickness / diameter, lift-off) and on magnetic parameters (magnetization curve of pipe and yoke / magnetic field strength of yoke)
Here only a subset of this multi-parameter space will be discussed:
The geometry of the setup and the diameter of the pipe are held constant. The diameter of the pipe is 300mm. The magnetizing setup, the angle of the pole piece and the gap between the pole piece and the pipe as well as the magnetizing field is held constant, such that realistic fields are measured in the gap between pipe and pole. Furthermore, the material parameters are constant. We chose a magnetization curve for some standard steel hoping that the used material parameters in the mill will not deviate too much. However, the magnetization curve is a sensitive parameter. Our investigations showed

e.g. that the MFL signal amplitude is directly proportional to changes in the saturation value of the magnetization curve.
The notch width, *a*, is varied from 0.2 to 1 mm. Here we only report the results of width=0.4mm; the notch width is of less influence. The notch depth, *b*, varies from 0.5 to 2 mm. Only longitudinal outside notches are discussed here. In addition, the notch length, *c*, is always 10 mm. The wall thickness of the pipe, *t*, is varied from 4 to 20 mm and the diameter, *d*, of the drilled hole ranges from 0.9 to 8.1 mm. The lift-off varies from 0.5 to 5 mm. Here we only display simulations for the case of the pipe end testing machine signals *S1* and *S2*.

3.2. MFL signals of notches

We first simulated the MFL signal of notch defects. As discussed above we keep the notch width, notch length, pipe diameter and pipe material constant; therefore we have three parameters (notch depth, wall thickness, lift-off) in the input and one (B_x) as the result. The result is plotted in
Figure 4. In addition to the solution $B_x=B_x(t,b)$ we have plotted three lines which indicate solutions for the case of constant relative notch depth of 5%, 10% and 20% with respect to the wall thickness. It is clearly seen that the MFL signal is increasing almost linearly (especially for small *t*) if notches with constant relative depth (e.g. 10%) are regarded. For the case of constant absolute value of notch depth the signal is decreasing with increasing wall thickness. In the investigated range (maximum defect size / notch depth is 10% - 50% of wall thickness) the MFL signal as a function of defect size (depth, *b*) is increasing linearly.

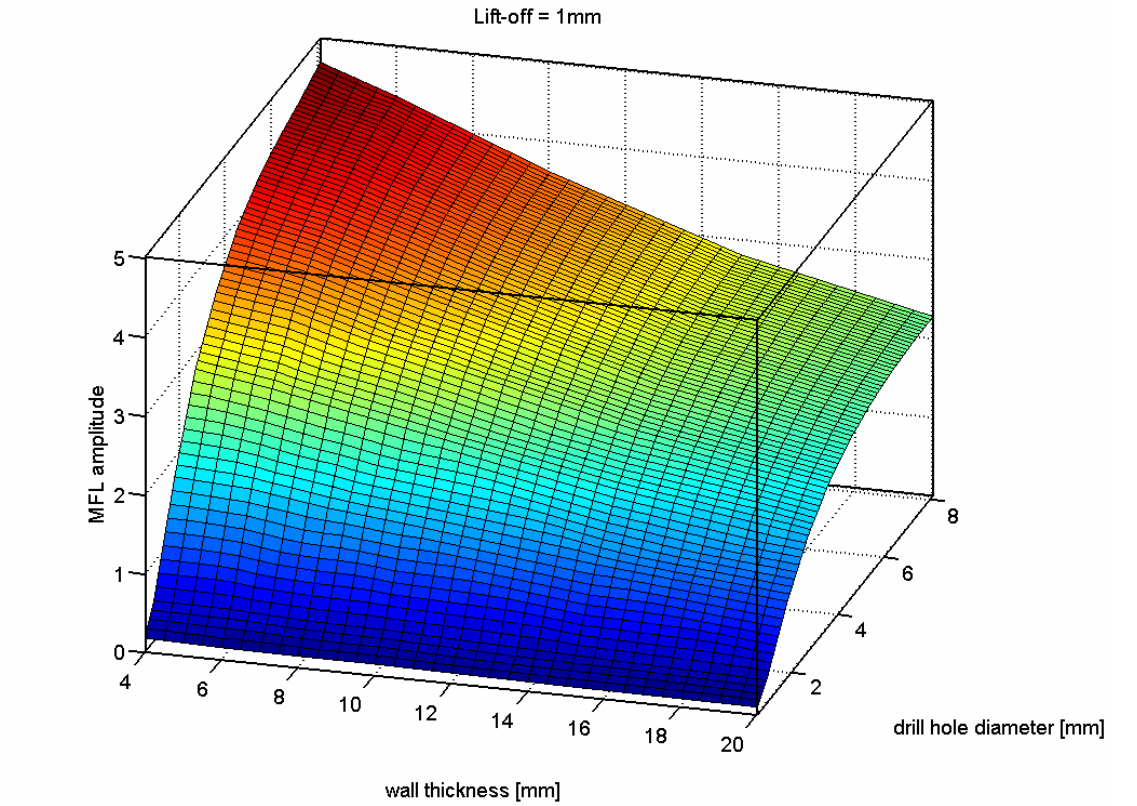

Figure 5: simulation results for the MFL signal $S1 = B_x$ [mT] as a function of drill-hole diameter, *d*, and wall thickness, *t*, for a lift-off of 1mm.

3.3. MFL signals of drill-holes

The same kind of FEM investigation was performed for the case of drill-holes as defects. The signal is calculated as a function of wall thickness, *t*, and in this case the hole diameter, *d*. The result is presented in *Figure 5*. As for the case of notches there is a decrease of *S1* as a function of wall thickness for constant defect size. However, the situation for constant wall thickness and increasing defect size *t* has changed: while starting linearly the MFL signal slope decreases at hole diameters around 5 mm.

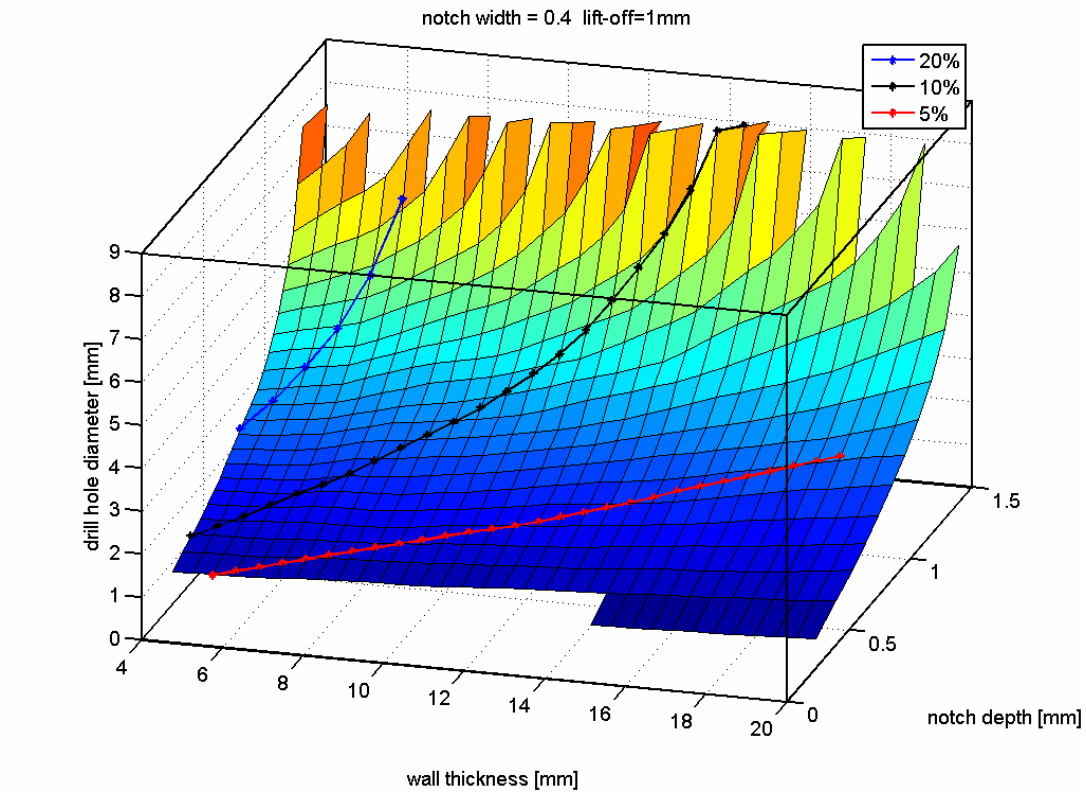

Figure 6: drill-hole diameter as a function of equivalent notch depth and wall thickness for the signal *S1*, i.e. lift-off = 1mm.

3.4. Notch-equivalent drill-holes

For calculating the drill-hole diameter which will exhibit the equivalent signal as some notch, it is clear, that this has to be done separately for different notch width and length, material and magnetizing setup properties, etc. Here we only present and discuss the special case which is characterized in section 3.1. In a first step the two results from the FEM calculations reported in

Figure 4 and *Figure 5* have to be inverted numerically. The following computations were carried out using MATLAB [5] making intensive use of build-in functions for data-griding and triangulation. We start by interpolating the results onto a common regular grid spanning the wall thickness and MFL signal subspace, (*S1*, *t*). This results in two mappings $(S1, t) \rightarrow b$ and $(S1, t) \rightarrow d$.

Because the grid (*S1*, *t*) is chosen identical for the two mappings it is possible to substitute the *S1* part of the grid, such that a new mapping $(b, t) \rightarrow d$ is obtained. This is only possible for those regions where the signals *S1* in the two initial FEM calculations have a common set of values. The result is plotted in *Figure 6* for 1mm lift-off. The

figure also shows the lines of relative notch-depth with respect to wall-thickness. It can be seen, that for larger values of the notch-depth the equivalent drill-hole diameter is increasing very fast, and for a notch depth above ~1.3 mm no reasonable drill-hole diameters are obtained. Furthermore, if regarding relative notch-depth values it is seen that only for the 5% notch reasonable drill-hole diameters are obtained for a larger wall-thickness regime. The larger notches of 10% or even 20% notch-depth do only have corresponding drill-hole diameters for very small wall-thicknesses.
The same calculation is applied to the signals *S2* (higher lift-off). The results are displayed *Figure 7.*

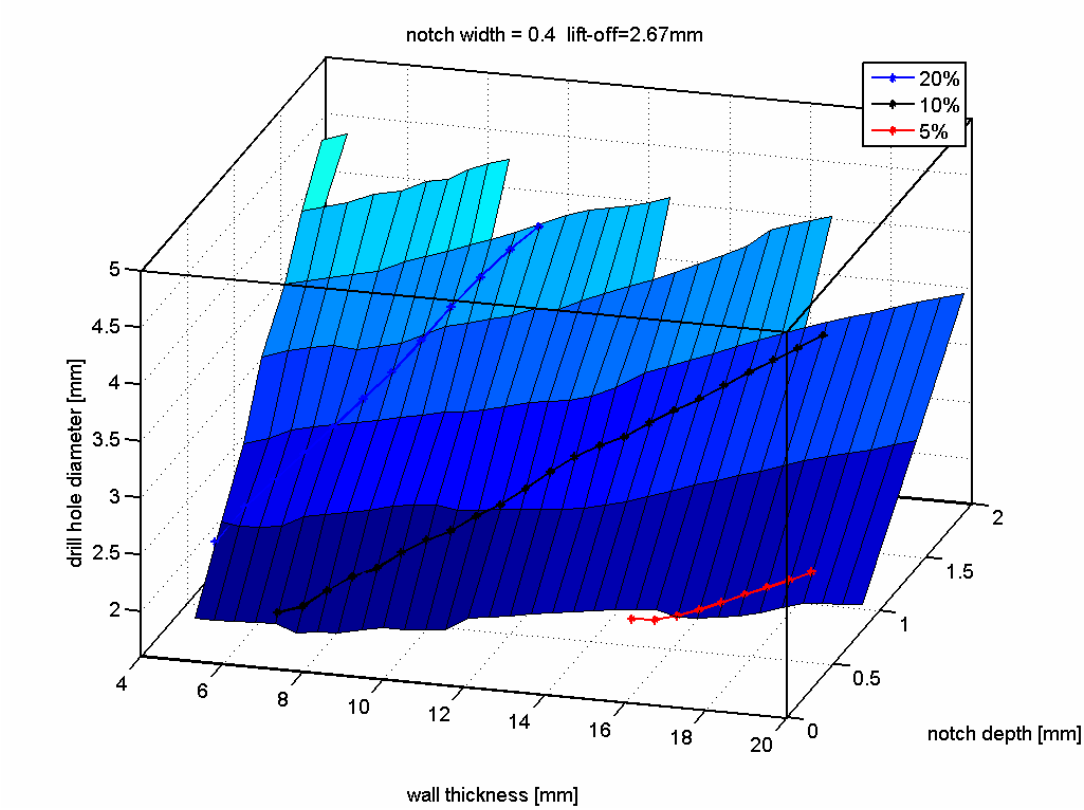

Figure 7: drill-hole diameter as a function of equivalent notch depth and wall thickness for the signal *S2*, i.e. lift-off = 2.67mm.

It is clearly seen that the surface spanned by the mapping $(b, t) \rightarrow d$ is quite different for the two cases depicted in *Figure 6* and *Figure 7*. Thus, the lift-off of the sensor is a very important parameter in this calculation influencing not only the absolute value of the equivalent drill-hole diameter, but also the shape of the function.
The behaviour for the signal *S2* is generally more linear and it possible to find corresponding drill-holes for comparably larger notches. In particular, the 10% notches have reasonable corresponding drill-holes (~2 to 4.5 mm) over a larger range of wall-thickness (~6 to 18 mm). It should be mentioned here, that these ranges here are limited through the range of the calculation performed. It is obvious that extending the calculations to smaller and higher wall-thicknesses will increase the range of correspondence given above.

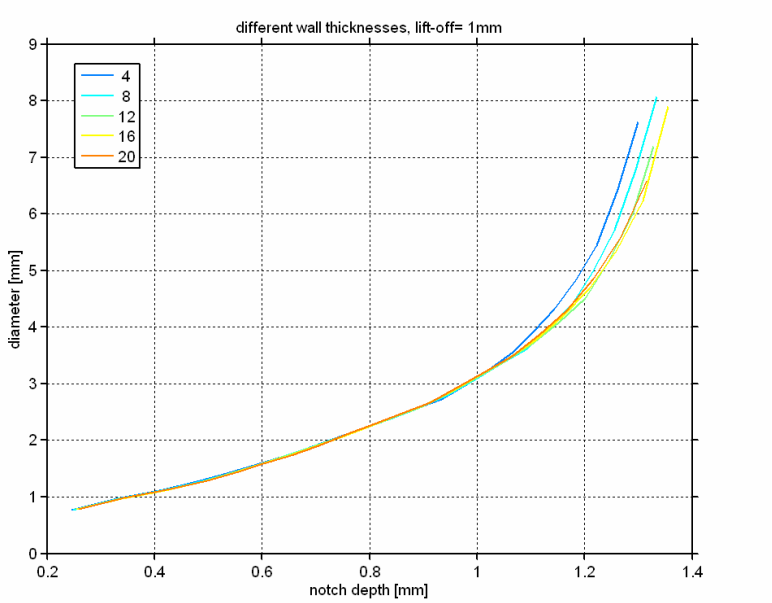

Figure 8: lines of equivalent drill-hole diameters as a function of notch depth for the signal *S1* (left, lift-off = 1mm) and several wall thicknesses (given in the insets).

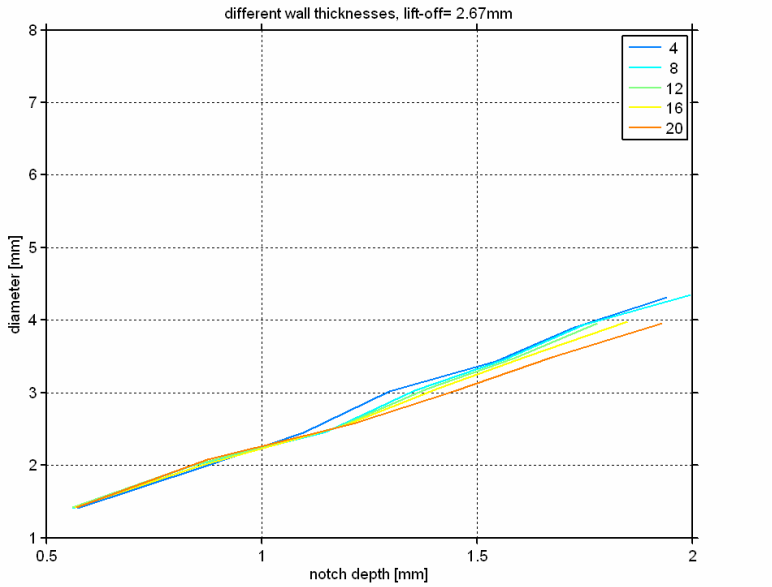

Figure 9: lines of equivalent drill-hole diameters as a function of notch depth for the signal *S2* (right, lift-off = 2.67 mm) and several wall thicknesses (given in the insets).

In general, the signal *S1* (*Figure 6*) is better suited for smaller notches and the signal *S2* (*Figure 7*) is more useful for larger notches.
In addition, the equivalent drill-hole diameter as function of absolute notch depth is plotted for different wall thickness for both lift-off values (*S1* and *S2*) in *Figure 8* and *Figure 9*. These functions show a very remarkable behavior. It is observed that the dependance of drill-hole diameter as a function of absolute notch depth is almost

independant of the wall-thickness, which is obviously very nice for pratical considerations.

4. Conclusions

We have shown that the proposed fast recalibration procedure using drilled holes as reference for MFL is principally possible but has a limited range in terms of notch-depth and drill-hole diameter. This range strongly depends on the lift-off of the sensors: for a relative notch depth of 10% of the wall-thickness a lift-off of 2.67mm is better suited than smaller lift-off values. The curves of corresponding drill-hole diameter as a function of notch-depth show a remarkable independency of the wall-thickness of the tube.
It is very important to note that the presented calculations are only valid in the parameter range discussed. In particular, the ferromagnetic material properties may be of high relevance.

References

[1] ORTH, T.; KAACK, M.; NITSCHE, S.; DELHAES, C.: Einsatz von neuen Magnetfeldsensoren zur Streuflussprüfung an nahtlosen Stahlrohren. In: DGZfP Berichtsband, 2005, P40

[2] SCHMITTE, T.; NITSCHE, S.; GROOS, A.: Modeling of Magnetic Flux Leakage Measurements of Steel Pipes. In: Conference Proceedings ECNDT, 2006, P98

[3] KAACK, M.; ORTH, T.; FISCHER, G.; WEINGARTEN, W.; KOKA, A.; NITSCHE, S.; ARZT, N.: Neue Rohrendenprüfung für nahtlose Stahlrohre. In: DGZfP Berichtsband, 2008

[4] www.comsol.com

[5] www.mathworks.com